ORIGINAL

The effect of elevated temperature exposure on the fracture toughness of solid wood and structural wood composites

Arijit Sinha · John A. Nairn · Rakesh Gupta

Abstract Fracture toughness of wood and wood composites has traditionally been characterized by a stress intensity factor, an initiation strain energy release rate (G_{init}) or a total energy to fracture (G_f). These parameters provide incomplete fracture characterization for these materials because the toughness changes as the crack propagates. Thus, for materials such as wood, oriented strand board (OSB), plywood and laminated veneer lumber (LVL), it is essential to characterize the fracture properties during crack propagation by measuring a full crack resistant or R curve. This study used energy methods during crack propagation to measure full R curves and then compared the fracture properties of wood and various wood-based composites such as, OSB, LVL and plywood. The effect of exposure to elevated temperature on fracture properties of these materials was also studied. The steady-state energy release rate (G_{SS}) of wood was lower than that of wood composites such as LVL, plywood and OSB. The resin in wood composites provides them with a higher fracture toughness compared to solid lumber. Depending upon the internal structure of the material, the mode of failure also varied. With exposure to elevated temperatures, G_{SS} for all materials decreased while the failure mode remained the same. The scatter associated with conventional bond strength tests, such as internal bond and bond classification tests, renders any statistical comparison using those tests difficult. In contrast, fracture tests with R curve analysis may provide an improved tool for characterization of bond quality in wood composites.

Introduction

Understanding of fracture in wood and wood composites is important because internal flaws (such as cracks) can lead to failure before the ultimate load capacity is

A. Sinha (✉) · J. A. Nairn · R. Gupta
Department of Wood Science and Engineering, Oregon State University, Corvallis, OR, USA
e-mail: arijit.sinha@oregonstate.edu

reached as determined by stress criteria (Anderson 2005); this effect can cause traditional stress design methods (AFPA 2007) to give poor predictions of load-bearing capacity. Structures that have tensile stress perpendicular to grain direction are of particular concern. An alternative approach to analyzing these cracks is to use fracture mechanics. Traditionally, fracture mechanics methods use one of two methods—stress intensity factor or energy release rate (Anderson 2005). For fiber-reinforced composites (and by analogy for wood and wood composites), energy release rate methods are more useful than stress intensity methods (Anderson 2005). In this method, the energy required to initiate and propagate a crack is called the fracture toughness and it can be measured during stable crack growth tests. In many materials, resistance to fracture increases as the crack grows. This increase after crack growth is due to the development of a process zone (Morel et al. 2003; Smith and Vasic 2003; Nairn 2009). A process zone in wood and wood composites is usually the result of fiber bridging. When a crack propagates, some non-fractured fibers cross the crack surface in the wake of the crack; these bridged fibers continue to carry stress and will increase the failure load compared to a material with stress-free fracture surfaces. As a result, the toughness increases as a function of crack length. Experimental observation of this increase is known as the material's fracture resistance or R curve (Fig. 1c).

Conventional fracture mechanics methods have been applied to wood starting in 1960s (Wu 1963, 1967) and has been reviewed by Vasic (2000), Smith et al. (2003) and Stanzl-Tschegg and Navi (2009). Most studies have focused on either initial fracture toughness (G_{init}) (Stanzl-Tschegg and Navi 2009; Aicher 2010) or total energy (G_f) at fracture (Frühmann et al. 2002b; Reiterer et al. 2002a, b). Neither of these methods provides a full fracture characterization. G_{init} is a useful material property, but the initiation toughness ignores contributions to material properties from fiber-bridging zones. G_f is approximately a measure of area under R curve, but it provides no information about the shape of the R curve. For example, some specimens may never reach G_{SS}, and such materials are not well characterized by an average value for an unknown extent of process zone development. An additional complication is that edge effects can lead to artifacts in total fracture energies (Matsumoto and Nairn 2012). An improved way to characterize fracture properties of wood and wood composite is to record the complete R curve. If a material reaches G_{SS}, the results provide G_{init}, G_B, G_{SS} and the size of the bridging zone. If a specimen does not reach G_{SS}, the shape of the rising R curves can still provide information about fiber-bridging processes such as the bridging stress (Matsumoto and Nairn 2012).

Wood is an orthotropic material, with three planes of symmetry namely longitudinal (L), tangential (T) and radial (R) (Green et al. 1999), giving rise to 6 directions of possible crack propagation, namely, RL, TL, RT, LR, LT and TR. The second letter represents the direction of crack propagation, while the first letter indicates the direction normal to the crack plane. Prior work has looked at crack propagation in all 6 directions (although results in LR and LT are suspect because cracks generally will not propagate in these directions) (Stanzl-Tschegg and Navi 2009). Two structurally important paths are RL and TL crack growth along the wood fibers. Prior studies characterizing RL and TL direction toughness, such as Schniewind and Centeno (1973), Johnson (1973) using stress intensity, and
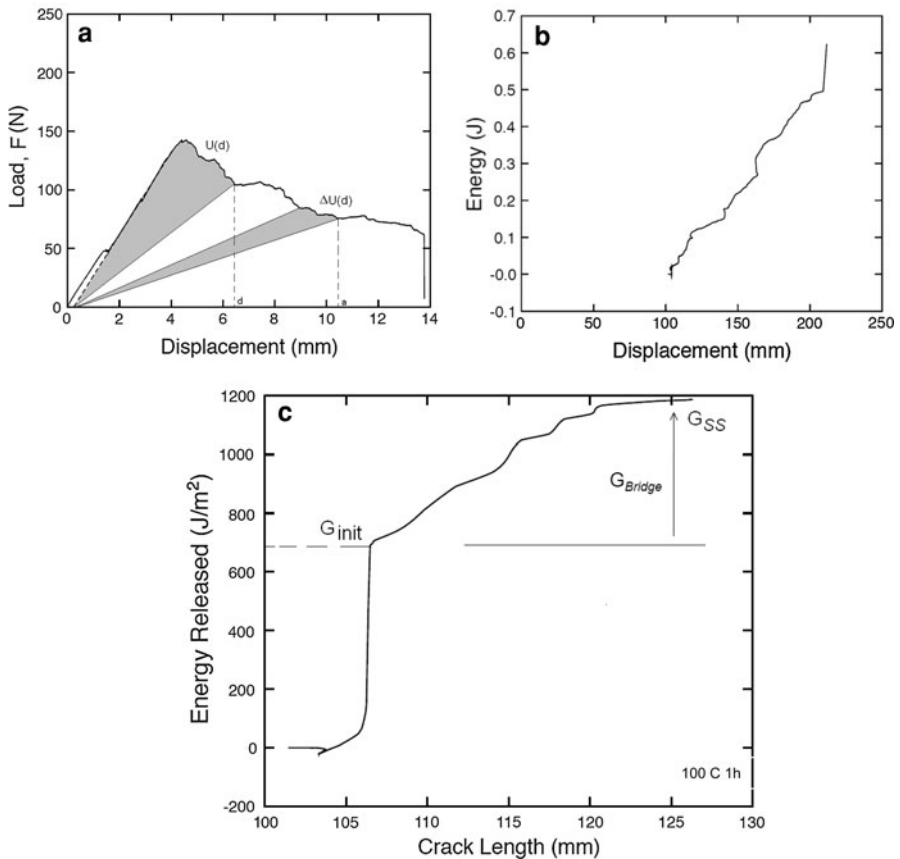
Fig. 1 *R* curve analysis procedure: **a** Typical load displacement curve. The *left shaded area* is total energy released up to displacement *d* (*U*(*d*) from Eq. 3). The *right shaded area* ɩσ an increment in released energy (Δ*U*ₓ(*d*) for Eq. 2); **b** Total energy released per unit thickness as a function of crack length; **c** *R* curve evaluated from slope of energy curve in **b**

Frühmann et al. (2002b) and Reiterer et al. (2002a, b) using total energy, are conflicting. A much clearer picture emerges when a complete *R* curve is used instead. Matsumoto and Nairn (2012) looked at RL and TL *R* curves in Douglas fir. The initiation values are similar and probably the same within experimental uncertainty (G_{init} = 158 J/m^2 for RL and 215 J/m^2 for TL). The *R* curves, however, were dramatically different. The RL *R* curve was essentially flat, while the TL *R* curve increased indicating TL direction has a higher toughness than RL. The results indicate that latewood zones provide bridging that enhances TL toughness. This conclusion is based on much larger differences than seen in prior work that did not record the full *R* curve. The new *R* curves for DF (described below) agree with these recent *R* curves.

Wood composites can also be studied by fracture mechanics (Conrad et al. 2004), although they have been studied less often than solid wood. A misconception in both synthetic and wood composites is that fracture mechanics may not apply.

Because fracture mechanics is simply energy balance during crack growth (i.e., thermodynamics) it must apply. The use of fracture mechanics, however, requires a material that can grow a crack and experiments that can monitor that crack growth—a situation that may not always exist in composites or may only exist for a few crack paths. Cracks in composites, like medium density fiberboard (MDF) and particle board (PB), can propagate either in- or through-the-thickness cracks (Matsumoto and Nairn 2007, 2012). It is a challenge to see these cracks but that issue can be solved with advanced imaging methods (Matsumoto 2009). In composites, such as OSB and plywood, only through-the-thickness crack propagation is possible. For LVL, crack propagation is easiest in the wood fiber direction. The crack surface may be parallel to the veneers (through-the-thickness cracks) or perpendicular, but most work has focused on the former. As in solid wood, most prior fracture work has used either conventional fracture mechanics for crack initiation or looked at total fracture energy. Niemz and Diener (1999) measured K_{Ic} for initiation in chip board, MDF, PB, OSB and plywood. They looked only at initiation. Ehart et al. (1996, 1998, 1999) studied PB and parallam (PSL) by total work of fracture using initiation and total area under the force–displacement curve, rather than a full R curve analysis. Mihashi and Hoshino (1989) supported the use of R curve analysis in fracture mechanics of LVL to verify their experimental results with analytical solutions. Recently, Matsumoto and Nairn (2007, 2012) characterized fracture properties of MDF and PB with a full R curve analysis. They observed large fiber-bridging effects; thus, the characterization of wood composites, like solid wood, requires a full R curve analysis (Nairn 2009). The results here extended the methods of Matsumoto and Nairn (2007, 2012) to experiments on OSB, plywood, LVL and solid wood. The authors are not aware of prior R curve studies on OSB or plywood. Fracture properties of these wood composites will depend upon the fracture properties of the adhesive bond, fracture properties of the wood phases and potentially on voids spaces (especially in OSB) (Conrad et al. 2004).

This study used energy methods during crack propagation to measure full R curves for comparing the fracture properties of solid wood and various wood-based composites such as, OSB, LVL and plywood. The materials were then exposed to 100 or 200°C for one or 2 h. The R curves before and after exposures were used to study the effect of elevated temperature on fracture properties. A side objective was to study if fracture testing might be preferred over conventional bond strength tests, such as IB and bond classification tests. The authors thus also looked at bond strength tests before and after exposure to elevated temperatures. The observed changes to the fracture properties versus bond strength properties helped to assess the efficiency and sensitivity of the two methods for wood composites.

Materials and methods

Materials

The fracture properties of six different materials were evaluated—Douglas fir (*Pseudotsuga menziesii*) solid sawn lumber, laminated veneer lumber (LVL),

plywood (2 thicknesses) and Aspen oriented strand board (OSB, 2 thicknesses) (see Table 1). To observe thermal effects, all materials were exposed to two elevated temperatures: 100 and 200°C. At each temperature, the materials were exposed to two different exposure times: 1 and 2 h. These conditions resulted in five different heat treatments, namely, control (CTRL), 100°C-1 h (100C1), 100°C-2 h (100C2), 200°C-1 h (200C1) and 200°C-2 h (200C2). This study was a part of greater study on thermal degradation of structural lumber in a protected timber-frame structure (Sinha 2010). As part of the study, the elevated temperatures were chosen to correspond to pre-charring temperatures that might occur in a protected timber-frame structure. Moreover, the structural design code for timber construction (AFPA 2007) requires a structure to meet either 1 or 2 h fire ratings. Hence, the exposure time of 1 and 2 h was chosen. All specimens were conditioned to equilibrium moisture content (EMC) prior to exposure to temperature. The samples were then heat treated in a convection oven. For each treatment, the oven was preheated to the desired temperature, as monitored by both internal and external thermo-couples. Once the desired temperature was reached, the samples were placed in the oven for the designated exposure time. After removal from the oven, the specimens were cooled to room temperature and then tested (without moisture re-equilibration). The observed property changes may represent the combined effects of changes due to moisture change and due to exposure to elevated temperature.

Specimens from all materials and exposure conditions were tested for fracture properties. The plywood and OSB specimens were additionally tested for bond strength. Because fracture propagation experiments generate many data points from each specimen and the image processing and subsequent R curve analysis was time intensive, only 2 samples for each material per treatment were tested for crack propagation, making it a total of 60 fracture tests. For IB and Bond classification tests, a sample size of 26 was used. This size was chosen, based on a pilot study,

Table 1 Details of various materials with their respective symbols, densities and dimensions

Material		Symbols	Density (g/cm^3)	Specimen size			Sample size		
				L (mm)	B (mm)	t (mm)	Fracture	IB	Bond class
M1	Solid sawn lumber	SSL	0.487	254	25.4	25.4	10		
M2	Laminated veneer lumber	LVL	0.512	254	90	38	10		
M3	Oriented strand board	OSBH	0.592	254	76	11.9	10	130	
M4	Oriented strand board	OSBO	0.543	254	76	22	10	130	
M5	Plywood	PWH	0.503	254	76	11.2	10		130
M6	Plywood	PWO	0.468	254	76	24	10		130
Total							60	260	260

such that an alpha priori level of 0.05 may be achieved in statistical tests for comparison between treatments.

Testing methods

Fracture

The fracture tests were conducted on double cantilever beam specimens (DCB). The specimen size and thickness for all the materials are listed in Table 1. The fracture set up is shown in Fig. 2. Two L-shape steel channels connected to compression grips were used to load the specimen ends at a rate of 2 mm/min. The DCB specimen was supported at the opposite end with a metal plate. A notch was created for the L channels to fit into the DCB specimen. The notch length on either arm was 25.4 mm so that a proper grip is ensured and eccentric loading is avoided. The notch was followed by a pre-defined, initial crack of 76 mm in length. The material itself determined the thickness. The width was chosen similar to composite delamination specimens. The length was chosen to allow observation of steady-state crack propagation prior to interference by edge effects. The load, deflection and time data were recorded using an Instron 5582 data acquisition system.

An important need for energy methods, especially for R curve analysis, is accurately tracking crack growth during the test. This was achieved by optical methods. A pair of CCD cameras was used to track the crack propagation by sequential image capturing at a rate of 2 per second (which was automated using ViC Snap software) with a time stamp. Similarly, analog load and deflection data were obtained from the Instron 5582 with a time stamp. Because the loading and image capturing were started simultaneously, the two time stamps coincided with

Fig. 2 Experimental set up for experiments on double cantilever beam specimens. The cameras record images for later determination of crack length
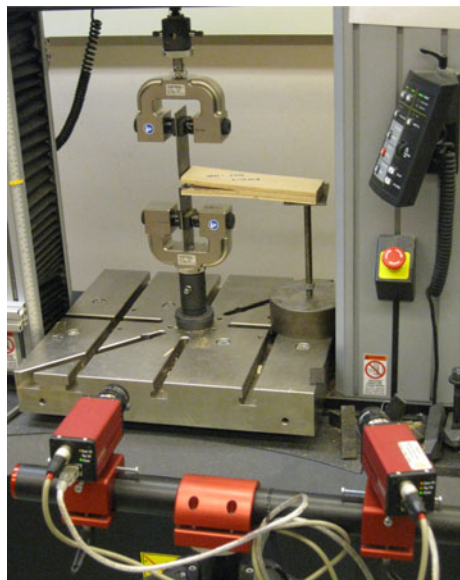
each other allowing correlation between load, deflection and image number. The images were then analyzed using ImageJ, by first, calibrating each set of images against measured dimensions in pixel coordinates. Then, the crack growth was visually tracked in pixel coordinates, which were converted to units of length (mm). The crack length was tracked only on the surface. Because the energy analysis below only needs crack growth (and not absolute crack length), surface tracking is sufficient even if the internal crack front is not straight. An advantage of using two cameras is that it provided a stereoscopic view and verification for the results between cameras. The second camera was used to verify the results and it matched the crack length calculations from the first camera. The final, raw experimental results were curves for load and crack length versus deflection, which were analyzed to determine the R curve by methods described in the next section.

R Curve analysis

The R curve is defined as the actual amount of energy released as a function of the extent of crack propagation:

$$R(\Delta a) = G_{\text{init}} + G_{\text{B}}(\Delta a) \tag{1}$$

where G_{init} is the initiation toughness and $G_{\text{B}}(\Delta a)$ is the toughness due to bridging, which depends on the amount of crack growth, Δa. In materials with fiber bridging, R starts at $R(0) = G_{\text{init}}$ and $G_{\text{B}}(0) = 0$. As the crack propagates, R increases as the fiber-bridging zone develops, which causes $G_{\text{B}}(\Delta a)$ to increase. If the crack propagation is sufficient long (e.g., in large specimens) or the bridging zone is sufficient short, $G_{\text{B}}(\Delta a)$ may reach a constant value. When this constant value is reached, the R curve will plateau at a constant toughness denoted here as steady-state toughness or $G_{\text{SS}} = G_{\text{init}} + G_{\text{B}}$, where G_{B} is the total toughness associated with a fully developed bridging zone. The rising part of the R curve corresponds to crack tip propagation while the edge of the process zone remains stationary at the initial crack tip (the notch root). During this phase, the process zone is increasing in length. Steady-state crack propagation occurs when the crack tip and notch root propagate simultaneously. In this regime, the fiber-bridging zone is fully developed and remains constant in length (Nairn 2009). Figure 1c shows a typical R from these experiments. This R curve for LVL starts with G_{init} of about 700 J/m^2, rises for about 15 mm of crack growth and reaches G_{SS} of about 1,200 J/m^2, which implies G_{B} of about 500 J/m^2.

   The method used in this study is direct experimental evaluation of R curve based on careful experiments for both force and crack length as a function of displacement. During fracture experiments, energy is released as the crack propagates through the material. A typical load deflection curve from theses results is shown in Fig. 1a. The load increases to a peak load, P_{max}, and then decreases as the crack propagates. The R curves or toughness, $G_{\text{IC}}(a)$, as a function of crack length can be determined from the load deflection curve using:

$$R = G_{\text{IC}}(a) = \frac{\Delta U_f(a)}{t.\Delta a} \tag{2}$$

where t is the thickness of the material, Δa is the crack growth and $\Delta U_f(a)$ is the energy released for the crack increment (see shaded triangular area to the right in Fig. 1a). Effectively, each increment in crack length can be treated as a separate test providing a new result. This analysis assumes the fracture process is elastic because it assumes the unloading lines return to the origin. An experimental result on different wood composite with fiber bridging has shown that this assumption is a good one (Matsumoto and Nairn 2012). An alternative method used in some composites fracture is to periodically unload the specimen to observe unloading (Hashemi et al. 1990). The problem with this method in fiber-bridging materials is that the unloading may break the fibers and thereby change the properties and the R curve (Atkins and Mai 1985). The preferred approach, and the approach used here, is to avoid unloading. In this approach, an elastic process assumption, when appropriate, is needed.

A second problem with Eq. 2 is that calculation of G_{IC} requires division by Δa (Eq. 2), which may be of very small magnitude, which leads to high scatter in the discrete increments in energy (Hashemi et al. 1990). In this study, a new method developed by Nairn (2009) was used to convert experimental results to continuous R curves. This revised area method helps to reduce the scatter by effectively smoothing energy and crack length experiments and finding slopes from full curves rather than point-by-point as in Eq. 1. The method is a four-step process. First, load and crack length versus displacement data sets are obtained as described above. Second, the force–displacement data are transformed to a total energy released curve by integrating the area under the curve up to some displacement, d, and then subtracting the remaining stored energy by extrapolating back to the origin. This area at one d is shown to the left in Fig. 1a; it is defined by:

$$U(d) = \frac{1}{t}\left(\int_0^d F(x)\,dx - \frac{1}{2}F(d).d\right). \tag{3}$$

Third, this cumulative energy is re-plotted as a function of crack length by inverting a smoothed crack length curve, $a(d)$, to find crack length for any given displacement. A sample $U(a)$ curve is shown in Fig. 1b. By Eq. 1, the slope of this curve is the toughness as a function of crack length. Thus, the fourth step is to numerically differentiate $U(a)$ to find R or $G_{IC}(a)$; a typical result is in Fig. 1c. A material that obeys classical fracture mechanics will have a constant slope $U(a)$ or a linear result. A material with a rising R curve will have a curved $U(a)$ result that is convex up. The slope of $U(a)$ as a function of a gives an experimentally determined and continuous R curve from the raw input of force and crack length at synchronized displacements. As shown in Fig. 1c, the R curve can be characterized by an initiation value (the start of the R curve or G_{init}) and a rising region. If the crack propagation process reaches steady state, the plateau value is termed the steady-state toughness, G_{SS}. The difference between G_{SS} and G_{init} is the toughness associated with bridging effects, G_B. Note again that this method directly measures $R(a)$ and therefore does not depend on any assumptions about bridging laws. The only assumption is that the overall process is elastic (this assumption leads to the second

term in the integrand in Eq. 3), and this assumption appears good for wood composites (Matsumoto and Nairn 2012).

Internal bond

Internal bond strength for OSB (OSO and OSH) was determined according to ASTM (2005) Standard D-1037. The OSB was cut into 50 mm square samples. Both surfaces were glued to aluminum alloy loading blocks. The blocks were secured in the testing apparatus, and a tensile force was applied at a speed of 1 mm/min until failure. The peak stress at failure (in MPa) was used to assess the internal bond strength. At each treatment, 26 samples were tested, giving a total of 130 samples for each material.

Bond classification for plywood

The bond classification test for plywood, as outlined in PS-1 (NIST 2007), involves testing of 25.4 mm square test area in the center of the specimen. The specimens were cut to specification of PS-1 (NIST 2007) to be 82.6 mm long by 25.4 mm wide and saw-kerfed one-third of the length of the specimen from each end, to provide the desired test area. The saw kerfs extended two-thirds of the way through the ply to be tested, and care was taken not to penetrate the next bond line. Specimens were oriented so that the grain direction of the ply under test runs at a 90° angle to the length of the specimen. These specimens were gripped and pulled at a rate of 2 mm/min. PS-1 only uses visual inspection of the percentage wood failure in the sample. Here both the percentage wood failure and maximum load at failure were recorded. A total of 260 samples were tested for two materials (PWH and PWO) consisting of 26 samples per material per treatment.

Results and discussion

Average results for G_{init} and G_{SS} for all material and all thermal treatments are in Table 2. The bridging toughness is the difference $G_B = G_{SS} - G_{init}$. Each value represents the average of two values (unless otherwise noted) as obtained from the measured R curves. Sample experimental R curves for LVL, solid sawn lumber, plywood and OSB are shown in Figs. 1 and 3. Also shown in Table 2 is the bridging zone length, which is the amount of crack growth required to reach steady-state toughness. The following sections discuss each material type.

Solid sawn lumber

For Douglas fir, the authors looked at crack growth along the fibers, which may be RL or TL or mixed specimen orientations were mixed (i.e., neither pure RL nor TL). The results in Table 1 are thus an average of RL and TL toughness. At room temperature, the initiation toughness was 150 N/m and it increased to G_{SS} of 195 N/m. These toughness values were unaffected by thermal treatments except for the

Table 2 G_{init} and G_{SS} (J/m^2) of all the materials as calculated by R curve analysis across all treatments

Material	Treatments														
	CTRL			100C1			100C2			200C1			200C2		
	G_{init} (J/m^2)	G_{SS} (J/m^2)	BL (mm)	G_{init} (J/m^2)	G_{SS} (J/m^2)	BL (mm)	G_{init} (J/m^2)	G_{SS} (J/m^2)	BL (mm)	G_{init} (J/m^2)	G_{SS} (J/m^2)	BL (mm)	G_{init} (J/m^2)	G_{SS} (J/m^2)	BL (mm)
SSL	150	195	20	145	215	18	180	215	20	163	205	13	100	110	23
LVL	**1050**	1050	23	**500**	500	19	350	775	13	500	925	20	**225**	225	18
PWO	575	1175	25	600	1105	25	650	700	30	325	450	25	188	310	20
PWH	750	906	13	600	625	17	650	675	7	100	600	10	400	450	7
OSH	325	950	23	950	1300	19	875	1500	13	850	1050	20	**800**	**800**	18
OSO	300	380	20	125	250	43	160	340	40	200	381	35	155	175	15

The BL column is the length of the bridging zone or the amount of crack length required to reach steady-state crack propagation

Numbers in bold indicate the curves did not rise
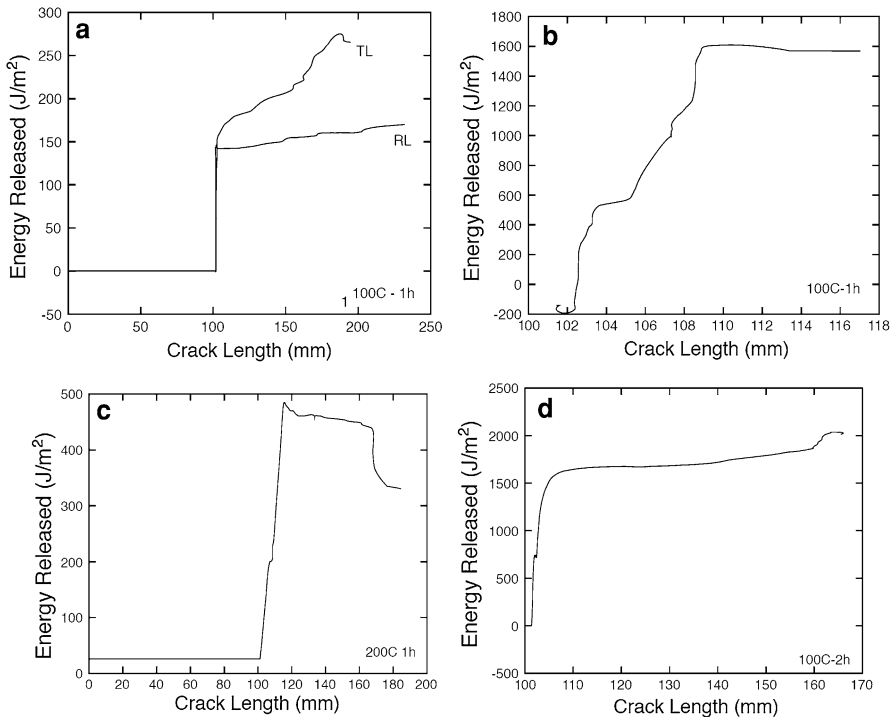
Fig. 3 *R* curves as a function of crack length for various materials tested at selected conditions. **a** SSL at 100C1, **b** PWO at 100C1, **c** OSO at 200C1 **d** OSH at 100C2. For sample LVL results, see Fig. 1

200C2 where G_{init} and G_{SS} dropped to 100 N/m and 155 N/m, respectively. Thus, solid wood is relatively unaffected by these thermal treatments except for the most severe conditions tested.

Prior fracture studies on Douglas fir or similar softwood species were limited either to initiation toughness or to total work of fracture. Schniewind and Centeno (1973) and Johnson (1973) measured initiation toughness at room temperatures, which can be compared here to G_{init}. Schniewind and Centeno (1973) and Johnson (1973) measured critical stress intensity factor, K_{Ic}, for initiation of RL and TL cracks in Douglas fir. Schniewind and Centeno (1973) found that K_{Ic} for RL to be higher than for TL (409 MPa $\sqrt{m}$ vs. 309 MPa $\sqrt{m}$). After converting their results to energy release rates (Matsumoto and Nairn 2012), Schniewind and Centeno (1973) reported G_{init} of 70 J/m^2 for RL fracture and 123 J/m^2 for TL fracture. Schniewind and Centeno (1973) concluded that radial ray cells, which are perpendicular to the crack plane in RL specimens, are arresting crack growth in the RL direction, but are not available to arrest crack growth in the TL direction. Johnson (1973) found the opposite or that TL toughness is higher than RL—G_{init} of 111 J/m^2 (374 MPa $\sqrt{m}$) versus for RL fracture and 84 J/m^2 (324 MPa $\sqrt{m}$) for TL fracture. He concluded, however, that the results were too close to draw conclusions. Yeh and Schniewind (1992) used a since abandoned J-integral method

to study initiation as a function of temperature, but not after high temperature exposure. They found $G_{init} = 300$ N/m at room temperature and observed a slight increase when heated to 60°C.

Most other prior studies looked at total work of fracture, G_f, measured only room temperature results and looked at species other than Douglas fir. As a result, direct comparison is imprecise. Although G_f might approximate an average toughness that could be analogous to G_{SS}, uncertain specimen and edge effects might change this relation. Prior observations of edge effects suggest that energy rises when a crack nears an edge, therefore G_f tends to be specimen dependent and higher than G_{SS} (Matsumoto and Nairn 2012). Here comparisons are restricted to other softwood species. Frühmann et al. (2002) and Reiterer et al. (2002a, b) used total fracture energy instead and compared RL and TL toughness for various species. Again, the results differ. Frühmann et al. (2002b) report G_f of spruce to be 180 N/m for RL and 230 N/m for TL, that is, higher toughness in TL than RL in both spruce and beech. They concluded the late wood zones, which are perpendicular to crack growth in TL specimens, are contributing to increased TL toughness. In contrast, Reiterer et al. (2002a, b) also for spruce found RL (337 N/m) toughness to be higher than TL toughness (213 N/m). Like Schniewind and Centeno (1973), they attributed the difference to rays cells inhibiting RL crack growth. They additionally measured initiation values of $G_{init} = 159$ N/m for RL and 84 N/m for TL (when their K_{Ic} results were converted to G_{init} using conversion factors for Douglas fir, which should be similar (Matsumoto and Nairn 2012)). Yoshihara and Nobusue (2008) looked only at initiation, but found results very close to Reiterer's total work of fracture—$G_{init} = 340$ N/m for RL and 220 N/m for TL.

Several papers looked at RT and TR fracture. RT fracture is the same fracture plane as RL fracture but the crack propagates in the tangential direction rather than the longitudinal direction. Similarly, TR fracture is the same fracture plane as TL but propagation is in the radial direction. Keunecke et al. (2007) calculated G_f for RT fracture of spruce and yew to be 290 and 310 N/m, respectively. For TR fracture, they observed unstable, slip-stick crack propagation as crack tips arrested within early wood zones and then periodically jumped through or even over late wood zones (see also Thuvander and Berglund 2000). Because of this unstable crack growth, G_f was expected to be a poor measure of toughness and was not reported. Similarly, Frühmann et al. (2003) focused on TR fracture, but because of slip-stick crack growth did not report toughness results for spruce.

Although the results of this study were mixed RL and TL direction (with some in between the two), the authors did identify some as pure RL or TL fracture. There was one condition (100C1) with both RL and TL fracture, and the separate results are plotted in Fig. 3a. The R curves are very different. For RL fracture, the R curve is essentially flat, which was attributed to easy crack growth predominantly within early wood zones. If fibers bridge these cracks, they do not carry much stress. In contrast, the R curve for TL fracture initiates at the same toughness by then increases with crack growth. This rise was attributed to bridging of the crack plane by latewood fibers. Indeed, the slip-stick process in TR fracture in the same fracture plane with cracks hopping over late wood zones (Thuvander and Berglund 2000) suggests a mechanism for late wood bridging effects. Matsumoto and Nairn (2012)

looked at RL and TL R curves in Douglas fir. The initiation values were similar when compared to existing literature. The R curves observed in this study and by Matsumoto and Nairn (2012) are different from those seen in the literature (Reiterer et al. 2002a, b). The RL R curve was essentially flat ($G_B = 0$) while the TL R curve increased to $G_{SS} = 620$ J/m², which implies $G_B = 405$ J/m² (Matsumoto and Nairn 2012). These new R curves for DF agree with these recent R curves. The results indicate that latewood zones provide bridging that enhances TL toughness. This conclusion is based on much larger differences ($G_B = 0$ versus 405 J/m²) than seen in prior work that did not record the full R curve. The results of this study agree with recent results by Matsumoto and Nairn (2012), although they saw larger bridging effects. The total contribution of bridging may be specimen dependent and the DCB specimens used here differed from the compact tension specimens used by Matsumoto and Nairn (2012).

In summary, when experiments reduce the toughness to a single value (either initiation or work of fracture), the results for all cited softwood species are within a narrow range of 70–340 N/m. Detailed comparisons between RL and TL planes or between two directions in the same plane (e.g., RL and RT) vary between studies. In other words, reducing toughness to a single value does not provide enough information to resolve details about fracture properties. In contrast, a complete R curve provides more information. When full R curves are recorded, for example, differences between RL and TL become clear and a likely mechanism (late wood bridging) can be postulated. Similarly, total work of fracture methods has been deemed unsuitable for slip-stick, TR crack growth (Keunecke et al. 2007; Frühmann et al. 2003). In contrast, an R curve could potentially track energy during the growth parts of TR crack growth with the challenge being to resolve such effects at the scale of growth ring dimensions. One recent result was able to observe a TR crack R curve in rapidly grown, Radiata pine, which had particularly large growth rings (>10 mm per ring). The R curve had step changes in toughness as it went through each early wood zone, but it is not known if the changes were due to a change in early wood toughness (e.g., from juvenile to mature wood) or to late wood bridging effects (Matsumoto and Nairn 2012). Finally, caution is needed if critical design scenarios are based on total work of fracture, G_f. Because specimen edge effects tend to increase G_f, such designs would be non-conservative. A potential solution is to use G_{SS} from the plateau of an R curve, provided that plateau is sufficiently removed from edge effects.

Wood composites at room temperatures

The G_{init} and G_{SS} for LVL, plywood (2 thicknesses) and OSB (2 thicknesses) are shown in Table 2. Among the wood composites, LVL was higher than plywood, which was higher than OSB. LVL, PWO and PWH are all laminated composites comprised of laminations running in the same direction (for LVL) and alternate directions (for plywood). These composites, even though they are fabricated primary from wood material, had considerably higher G_{init} and G_{SS} than SSL. The differences are likely due to a combination of resin effects and benefits of lamination in potentially inhibiting crack growth. The OSB composites were also

higher than SSL, but closer. Perhaps the short strands and/or different resin influence the toughness less than the laminations in LVL or plywood. There was some difficulty measuring full R curves in PWH, because the DCB arms were too thin. As a result, after crack initiation the arms tended to break resulting in no further crack propagation. The G_{init} results should be reliable, but the authors are not certain a true plateau was reached for measuring G_{SS}. Finally, the bridging zone lengths (see Table 2) were in the range of 7–43 mm, which overlapped the bridging zone lengths observed for SSL.

These experiments show that fracture mechanics methods can be used for a variety of wood composites and work especially well when a crack path is available—for example, between layers of LVL, PWO or PWH and between strands of OSB. Despite this fact, there are few crack probation studies for comparison. Frühmann et al. (2002a) reported G_{f} value of LVL between 280 and 333 N/m. This result is considerably lower than the G_{SS} value of LVL, which was 1100 N/m. Frühmann et al. (2002a) used aspen, which is a lower density wood, than Douglas fir and their specimen thickness was 12 mm while the LVL specimens here were 38-mm thick. The difference in results may also be due to the different testing protocols, that is, fracture mechanics versus total work of fracture. Niemz and Diener (1999) looked at plywood and OSB, but their cracks were in plane, they looked only at initiation (using stress intensity methods), and the failure did not achieve stable crack propagation.

Although the fracture properties of wood composites, such as LVL, plywood and OSB, have received little fracture mechanics study, there is much related work in the fracture mechanics of non-wood laminated composites. In this study, LVL and PWO are composites of laminated plies with a layer of adhesive between each ply. The G_{SS} values for LVL, PWO and PWH were five to seven times higher than SSL of the same species, where the SSL results taken are representative of the ply toughness. Sela et al. (1989) investigated the effect of adhesive layer between non-wood plies and observed a sevenfold–tenfold increase in the fracture toughness of the material due to an adhesive layer. Thus, the adhesive in wood composite provides benefit by increasing the composite toughness. In wood composites, the control values of LVL were lower than those of PWO (Table 2). These two composites differ by layup sequence, which has been shown to affect energy release rate of non-wood composites (Davidson et al. 2000; Lee and Knauss 2000; Anderson and Konig 2004). The critical energy release rate is generally higher for a multidirectional composite than a unidirectional composite (Davidson et al. 2000). Similarly, the multidirectional plywood (a cross-ply layup) showed higher toughness than LVL (unidirectional composite).

The G_{SS} for OSB were generally lower than for LVL and PWO. OSB is a strand-based composite, with various process parameters such as voids and undulations affecting its strength as well as the fracture toughness. Lei and Wilson (1980, 1981) found that fracture toughness of OSB was affected by void size and board densities while it was not affected by resin content or directionality of flakes. The inter-strand voids may act as flaws that aid in crack propagation. With more compaction, the board density is higher and there is less void space and hence higher toughness is expected. Conrad et al. (2004) suggested LVL represents perfectly bonded OSB,

therefore fracture toughness of LVL can be regarded as the upper bound for OSB. Although this argument has merit, perfectly bonded OSB, that is, no void space, will not have all the strands oriented in one direction. The core strands are either randomly oriented or oriented in cross-direction to the surface flakes and therefore might be more appropriately compared to multidirectional plywood rather than to LVL. Comparing G_{SS} between the two OSB types, OSBH has a higher G_{SS} than OSBO. The density of OSBO was lower than that of OSBH (Table 1), which may account for the lower toughness (i.e., due to more void space). The density difference might be because of higher compaction achieved by heat transfer during manufacturing of the OSBH than OSBO, due to their thicknesses (Zamborie et al. 2001).

Effect of elevated temperature

Table 2 lists the effect of exposure time on G_{init}, G_{SS} and bridging zone length (BL) at two temperatures of exposure for various materials. Solid sawn lumber (Fig. 3a) after exposure to 100°C has low toughness but it does not change much with time. After exposure to 200°C, there is little change after 1 h, but after 2 h both G_{init} and G_{SS} decrease (see Table 2). Wood is fairly stable at 100°C, especially for the exposure times used in this study. Hence, no detectable change was observed in G_{SS} of wood. When exposed to 200°C, however, wood deteriorates (Green et al. 1999; Sinha et al. 2011). The 43% decrease in G_{SS} of wood after 2 h of exposure at 200°C is a consequence of this thermal degradation. Yeh and Schniewind (1992) tested Douglas fir at temperatures ranging from 21 to 60°C and as a function of moisture content. They found that moisture had a more pronounced effect than temperature. They studied toughness at elevated temperatures, which differs from this study, which always measures room temperature toughness after thermal exposure.

For wood composites after exposure to 100°C, the results were scattered with no clear trends. As in solid wood, the authors claim this temperature had small effects on toughness. In contrast, after exposure to 200°C, G_{SS} for all materials dropped as the exposure time increased. The degradation in fracture toughness for wood composites can come from two mechanisms. First, wood starts to degrade in mechanical properties when exposed to 200°C (Sinha et al. 2011) as was observed here for SSL results. But wood composites initially have higher toughness due to resin contributions. Thus, thermal degradation of the resin can deteriorate its capacity to enhance toughness. Typical resins for wood composites tend to degrade after exposure to 200°C and degrade more at longer exposure time. Because of these combined mechanisms, the drop in G_{SS} after exposure to 200°C for 2 h, when compared with control values, is more for wood composites, such as PWO (73%), LVL (78%) and OSO (53%) than for SSL (43%). Furthermore, LVL and PWO are laminated composites and use higher resin content by weight than OSO, consequently, the drop in their respective G_{SS} values were the highest.

Failure modes and R curves

Selected R curves are shown in Fig. 3 while typical failure modes are shown in Fig. 4. The failure in SSL (Fig. 4a) is typically through one growth ring when

propagating in the RL direction. This failure mode leads to the flat R curve (as discussed above). In contrast, the R curve in the TL direction rises because the failure mode spans multiple growth rings and latewood zones can bridge the crack (Matsumoto and Nairn 2012). The failure mode for LVL was mostly fracture through the wood veneer sheets, with hardly any glue line failure (Fig. 4e). LVL is made up of high quality, relatively thick plies. Consequently, the crack can propagate through the ply starting from the initial crack. The corresponding R curve (Fig. 1c) initiates and then rises until it reaches a steady state. The rising R curve is a consequence of wood fibers that can bridge the crack plane within a veneer sheet (Nairn 2009). Frühmann et al. (2002a) observed a similar failure mode in aspen LVL. In plywood (PWO), fracture was a combination of ply delamination and ply fracture as shown in Fig. 4c and the corresponding R curve (Fig. 3b). The R curve is a stepwise curve representing ply delamination and ply fracture. The failure initiates at the ply and subsequent progression occurs by delamination and ply fracture. As the crack grows toward the end of the plywood specimen, it cuts across the plies and causes failure and delamination in the adjacent plies. Lee and Knauss (2000) observed a similar failure mode for non-wood, multidirectional composites. Failure in OSB, started as crack propagation along the strands with strand undulations governing the directions of crack growth (Fig. 4b). The void spaces acted as crack initiation points during advanced stages of loading and a discontinuous crack growth resulted, particularly in OSO. This trend is observed in the R curves, with

Fig. 4 Crack propagation failure modes for various materials. **a** Solid sawn lumber (SSL); **b** One-inch OSB (OSO); **c** Half-inch OSB (OSH); **d** One-inch plywood (PWO); **e** LVL

void spaces acting as localized crack initiation points resulting in energy going down as crack propagates (Fig. 3c). For OSH, which had less void space, a continuous crack could be identified (Fig. 4d) and the R curve reached a steady state (Fig. 3d). Overall, there was hardly any fracture through the strand thickness. The cracks found a plane of least energy for propagation, with strand undulation and void spaces helping in the fracture process, especially for OSO.

The failure surfaces of all the samples after 100°C treatments were essentially the same as the controls controls. After exposure to 200°C, toughness, G_{SS}, was much lower but the failure modes were again very similar, especially for plywood and OSB. The failure for LVL occurred mainly by crack propagation in veneer; however, glue failure was visible in one of the heat-treated samples. The failure in plywood was steady crack propagation with trans-veneer cracking and subsequent delamination. The OSB samples (OSO and OSH) exhibited identical failure characteristics to the control samples.

Because the rise in R curves depends on the development of the fiber-bridging zone, that rise is expected to be a specimen-dependent property. In contrast, the initiation value occurs before the process zone starts and therefore should be a specimen-independent property. The initiation values of this study were comparable to the initiation values by Schniewind and Centeno (1973) and Johnson (1973). If the fiber-bridging law is a material property than the steady-state value should be a material property as well (although the amount of crack growth required to reach steady state could depend on specimen type). The results here for both initiation and steady-state values results were close to results done using compact tension specimens by Matsumoto and Nairn (2012). In this paper, the emphasis was on the effect of temperature and not the details of the R curve. Since the focus was often put on G_{SS}, the only specimen requirement was that enough crack growth to reach steady state could be observed.

Internal bond and bond classification tests

The evaluation of bond strength in plywood is commonly done using a lap shear strength test called the bond classification test (NIST 2007). For OSB, the common bond strength test is the Internal bond (IB) test (ASTM D 1037). Both these methods have shortcomings. In the bond classification test, wood is loaded in shear parallel to the grain while in IB, it is loaded in tension perpendicular to grain. These are wood's two weakest orientations (Green et al. 1999). Both these tests typically have high scatter making it hard to find statistical significance in changes. Perhaps through-the-thickness crack propagation of plywood, OSB, MDF etc., would be a better test for bound quality? Fracture tests typically have less scatter and toughness may be a more fundamental failure property for internal bonds than transverse strength. Fracture testing of wood composites for the evaluation of wood adhesion is not a new concept (Gagliano and Frazier 2001; Ebewele et al. 1979, 1980, 1982, 1986). Most prior work, however, has looked at crack growth along an adhesive bond line between two layers of wood. This study explores whether fracture analysis of crack propagation within a single composite material (OSB, plywood, LVL, etc.) can be an alternative to conventional bond strength testing.
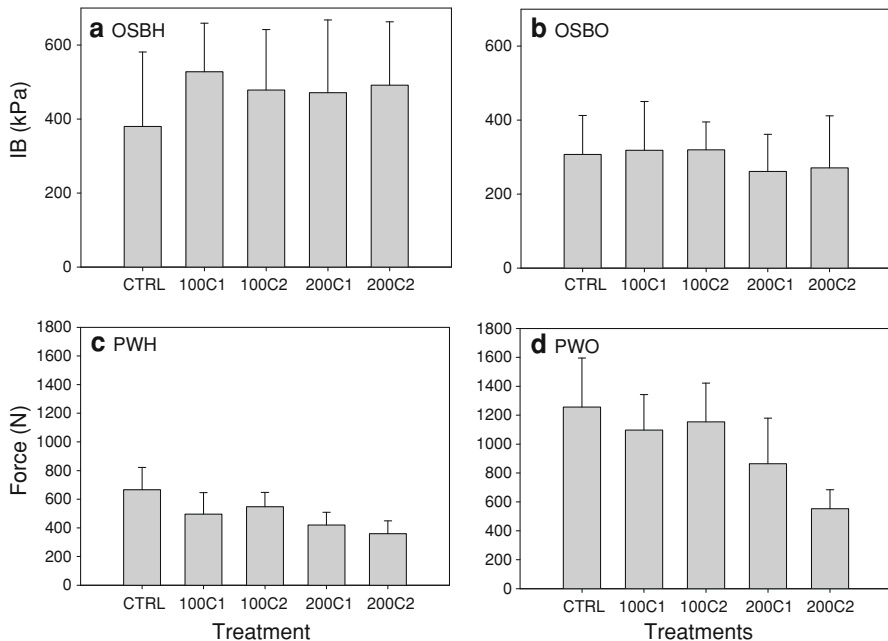
Fig. 5 Internal bond results for both thickness of OSB (**a**, **b**) and bond classification failure stresses for both thicknesses of plywood (**c**, **d**) for each of the test conditions

The IB and Bond Classification test results for OSB and PWH and all conditions in this study are shown in Fig. 5a–d. For both thicknesses of OSB, the IB tests had no effect on strength after exposure to elevated temperature. For plywood, tested by bond classification test, the property degraded with exposure to elevated temperature ($p < 0.01$, ANOVA), especially for both durations of the 200°C treatments. A drawback of IB testing when looking for statistically significant effects is the large scatter associated with IB results. The high scatter could be due to inherent variations in wood (River 1994) and due to drawbacks in the testing procedures (Gagliano and Frazier 2001). These conventional tests fail at statistically random weakest links. The theory of failure at weakest link holds true, but the weakest link can be anywhere from the adhesive between strands (which the test is intended to monitor), to void-initiated failure, weak internal strand failure, or glue line with the loading blocks. The weakest link is not pre-defined by the test protocol; hence, the coefficient of variation (COV) for IB test ranges from 25 to 40%. In this study, the COV for IB varied from 23 to 52%, which is typical for the test and highlights the problem when using this test to compare materials or conditions. With such variability, an assessment of the bond property with ample confidence cannot be made.

For bond classification, the PS1 (NIST 2007) requires observation of the percentage (%) wood failure while neglecting the maximum load at failure. However, load at failure is an important parameter as shown by Perkins (1950) and DeVallance et al. (2007). Here both maximum load and % wood failure were noted

Table 3 Percentage (%) wood failure in bond classification test for plywood (PWO and PWH)

Treatment	PWH (%)				PWO (%)			
	Average	SD	Min	Max	Average	SD	Min	Max
Control	74	25	0	100	57	19	20	100
100C1	70	25	20	100	53	22	20	95
100C2	65	21	20	100	53	24	10	95
200C1	48	28	5	100	42	23	5	95
200C2	50	28	5	100	19	20	0	90

(see Table 3). The average % wood failure decreased (i.e., % adhesive failure increased) after exposure to 200°C. For example, the average % wood failure for PWH decreased from 74% for control to 50% for 200°C-2 h of exposure. Similarly, for PWO, it decreased from 57 to 19%. The conventional test interpretation is that the bonding has degraded due to exposure. However, the failure could be a combination of degradation of wood and the adhesive. It is difficult to single out the degradation mechanism using these test results. However, it looks like the degradation in adhesive was governing the failure rather than bond properties especially in the treatments including a temperature of 200°C. A scenario now arises where the control and 100°C treatment samples have higher load and higher percentage of wood failure, while the 200°C treatment samples have lower load and lower percentage of wood failure. High % of wood failure accompanied by higher load at failure may not be a measure of the adhesive bonding rather than strength of wood. Contrastingly, there could be a scenario where higher % of wood failure occurs but the load at failure is low. This will be due to lower strength of wood rather than a measure of bond adequacy (Perkins 1950). Interpretation of bond classification tests leads to ambiguity in terms of what property is being measured; whether this is measure of adhesive strength or a wood property.

The IB test has problems with high scatter in the data rendering a statistical evaluation difficult. Here the scatter rendered IB results inadequate for detecting thermal degradation in OSB after exposure to elevated temperature. The bond classification test has lower scatter and was able to detect degradation after exposure to elevated temperature but is influenced by various other parameters, such as lathe checks (DeVallance et al. 2007). The bond classification, however, has ambiguity in terms of whether it is providing a measure of shear strength of wood veneers or the bond strength of adhesive. Although these tests are ingrained in the quality control process of manufacturing of OSB and plywood, they may not be ideal material characterization methods. The fracture tests here show that it is possible to grow cracks through both OSB and plywood and to measure toughness of that process. These crack paths are in the same failure planes as failure in IB and bond classification tests, but fracture methods might provide more fundamental, and therefore useful, material properties. A benefit of fracture testing is that it begins with a deliberate crack. Failure occurs at this crack and therefore such specimens are inherently less prone to scatter from a variety of failure sites. For the materials tested here, fracture testing was better able to detect changes in properties after

exposure to elevated temperature than either IB or bond classification tests. A draw back of fracture testing is that it is more time consuming than simple strength tests. The question remaining for research on OSB and plywood is: Is it better to run a few, challenging tests that may provide a fundamental failure property (fracture toughness or R curve) assessing adhesive and panel quality or to run many simple tests (IB on bond classification) that may have high scatter and ambiguous meanings?

A fracture test to characterize adhesive bonding is not a new concept. Much work has been done in this regard and has been reviewed by Conrad et al. (2004). However, fracture tests on a composite material as a whole, rather than on a specific bond line between two adherends, has not been extensively studied. Moreover, most prior fracture studies on wood used only stress intensity method, G_{init} or G_f to characterize fracture toughness. For a fiber-bridging material such as wood and wood-based composites, an R curve analysis is necessary to fully characterize the fracture properties. These fracture tests on the composite as a whole provide information on engineering material characteristics of the composite rather a specific adhesive bond line. The overall adhesive toughness and panel quality, however, will play significant roles in these properties such as the shape of the R curve and the plateau value for G_{SS}. These fracture tests were more demanding than IB or bond classification tests, in terms of time associated with data analysis and image processing. A goal of this research was to show that fracture tests can be done on OSB and plywood and provide useful results; the authors expect that further test development and automated image processing software could make the fracture tests easier.

Conclusion

Fracture properties of wood and wood-based composites were studied using experimental fracture methods. The authors were able to observe rising R curves for all materials by adapting a new analysis technique developed by Nairn (2009) and therefore to track thermal degradation in G_{init} and G_{SS}. The steady-state energy release rate (G_{SS}) of wood was lower than that of wood composites such as LVL, plywood and OSB. The resin in wood composites provides them with the higher magnitude of fracture toughness as compared to solid lumber. Depending upon the internal structure of the material, the mode of failure also varied. For laminated composites such as LVL and plywood, the modes of failure differed because of the different stacking sequences in the laminates. For LVL with unidirectional veneers, the mode of failure was crack propagation through the veneers, with hardly any glue failure. For plywood with cross-directional veneers, the failure was transverse ply cracking and delamination. For OSB, the void spaces influenced the crack propagation and failure pattern. The R curves for the composites and SSL had distinct features depending on their failure modes.

With exposure to elevated temperatures, G_{SS} of all the material decreased while the mode of failure was mostly unaltered. The highest drop in G_{SS}, however, was associated with the wood composites rather than solid lumber. The greater the resin

content in the composite, the greater was the drop. Hence, LVL and plywood had a greater drop in G_{SS} than OSB. The bond strengths for OSB and plywood were evaluated using IB and bond classification tests, respectively. The bond classification tests showed significant thermal degradation in bond strength of plywood but the IB tests were not able to detect degradation due to excessive scatter in the data. Additionally, it was unclear whether the IB or Bond classification provided a clear measure of adhesive bond strength. An alternative to IB and bond classification is presented in the form of fracture testing. The new fracture method, previously not applied to wood and structural wood composites, proved to be effective. This method may enable quality control and R&D personnel to adopt fracture methods for evaluation of wood composite panels.

References

AFPA (2007) National design specification® for wood construction. American Forest and Paper Association, Washington, DC

Aicher S (2010) Process zone length and fracture energy of spruce wood in mode I from size effect. Wood Fiber Sci 42(2):237–247

Anderson TL (2005) Fracture mechanics, fundamentals and applications. CRC Press: Taylor and Frances Group, Boca Raton, FL, pp 122–125, 310–311

Anderson J, Konig M (2004) Dependence of fracture toughness of composite laminates on interface ply orientations and delamination growth direction. Compos Sci Technol 64:2139–2152

ASTM D-1037-99 (2005) Standard test method for evaluating properties of wood-based fiber and particle panel materials. In: Annual Book of ASTM Standards. ASTM, West Conshohocken, PA

Atkins AG, Mai YW (1985) Elastic and plastic fracture. Wiley, New York

Conrad MPC, Smith GD, Fernlund G (2004) Fracture of wood composites and wood-adhesive joints: a comparative review. Wood Fiber Sci 36(1):26–39

Davidson BD, Gharibian SJ, Yu L (2000) Evaluation of energy release rate-based approaches for predicting delamination growth in laminated composites. Int J Fract 105:343–365

DeVallance DB, Funck JW, Reeb JE (2007) Douglas-fir plywood gluebond quality as influenced by veneer roughness, lathe checks, and annual ring characteristics. For Prod J 57(1–2):21–28

Ebewele R, River B, Koutsky J (1979) Tapered double cantilever beam fracture tests of phenolic-wood adhesive joints. Part I. Development of specimen geometry: Effects of bondline thickness, wood anisotropy, and cure time on fracture energy. Wood Fiber 11 (3):197–213

Ebewele R, River B, Koutsky J (1980) Tapered double cantilever beam fracture tests of phenolic-wood adhesive joints. Part II. Effects of surface roughness, the nature of surface roughness, and surface aging on joint fracture. Wood Fiber 12 (1):40–65

Ebewele R, River B, Koutsky J (1982) Relationship between phenolic adhesive chemistry, cure and joint performance. Part I. Effects of base resin constitution and hardener on fracture energy and thermal effects during cure. J Adhesion 14:189–217

Ebewele R, River B, Koutsky J (1986) Relationship between phenolic adhesive chemistry and adhesive joint performance; effect of filler type on fraction energy. J Appl Polym Sci 31:2275–2302

Ehart RJA, Stanzl-Tschegg SE, Tschegg EK (1996) Characterization of crack propagation in particleboard. Wood Sci Technol 30:307–321

Ehart RJA, Stanzl-Tschegg SE, Tschegg EK (1998) Crack face interaction and mixed mode fracture of wood composites during mode III loading. Eng Fract Mech 61:253–278

Ehart RJA, Stanzl-Tschegg SE, Tschegg EK (1999) Mode III fracture energy of wood composites in comparison to solid wood. Wood Sci Technol 33:391–405

Frühmann K, Tschegg EK, Dai C, Stanzl-Tschegg SE (2002a) Fracture behavior of laminated veneer lumber under mode I and III loading. Wood Sci Technol 36:319–334

Frühmann K, Reiterer A, Tschegg EK, Stanzl-Tschegg SS (2002b) Fracture characteristics of wood under
    mode I, mode II and mode III loading. Philosophical Magazine A: Physics of Condensed Matter,
    Structure, Defects and Mechanical Properties 82(17–18):3289–3298

Frühmann K, Burgert I, Stanzl-Tschegg SE, Tschegg EK (2003) Mode 1 fracture behavior on the growth
    ring scale and cellular level of spruce and beech loaded in TR crack propagation system.
    Holzforschung 57:653–660

Gagliano JM, Frazier CE (2001) Improvements in the fracture cleavage testing of adhesively-bonded.
    Wood Fiber Sci 33(3):377–385

Green DW, Winandy JE, Kretschmann DE (1999) Mechanical properties of wood. Pages 4:1–45 in Wood
    handbook, wood as an engineering material. Forest Products Society, Madison, WI

Hashemi S, Kinloch AJ, Williams JG (1990) The analysis of interlaminar fracture in uniaxial fibre-
    polymer composites. Proc R Soc Lond A 427:173–199

Johnson JA (1973) Crack initiation in wood plates. Wood Sci 6(2):151–158

Keunecke D, Stanzl-Tschegg SE, Niemz P (2007) Fracture characterization of yew and spruce in the
    radial-tangential and tangential-radial crack propagation system by micro wedge splitting test.
    Holzforschung 61:582–588

Lee S, Knauss WG (2000) Failure of laminated composite at thickness discontinuities under complex
    loading and elevated temperatures. Int J Solids Struct 37:3479–3501

Lei Y-K, Wilson JB (1980) Fracture toughness of oriented flakeboard. Wood Sci 12(3):154–161

Lei Y-K, Wilson JB (1981) A model for predicting fracture toughness of flakeboard. Wood Sci
    13(3):151–156

Matsumoto N (2009) The fracture toughness of medium density fiberboard and other fiber bridging
    composites. MS thesis, Oregon State University, Corvallis, OR

Matsumoto N, Nairn JA (2007) Fracture toughness of MDF and other materials with fiber bridging. In:
    Proceedings of the 22nd Annual technical conference of the American society of composites,
    September 17–19, Seattle, WA, USA

Matsumoto N, Nairn JA (2012) Fracture toughness of wood and wood composites during crack
    propagation. Wood Fiber Sci 42(2). http://www.swst.org/wfs/prePublication.html

Mihashi H, Hoshino M (1989) Fracture toughness and tension softening properties of glued laminated
    timbers. In: 8th European conference on fracture: fracture behavior and design of materials and
    structures, pp 799–804

Morel S, Mourot G, Schmittbuhl J (2003) Influence of the specimen geometry on R curve behavior and
    roughening of fracture surfaces. Int J Fract 121:23–24

Nairn JA (2009) Analytical and Numerical modeling of R curves for cracks with bridging zones. Int J
    Fract 5(2):167–181

Niemz P, Diener M (1999) Comparative investigations for the determination of fracture toughness at
    timber materials. Holz Roh- Werkst 57:222–224

NIST (2007) Voluntary Products Standard PS 1-2007. Construction and Industrial Plywood. Office of
    Standards Services, National Institute of Standard and Technology. Gaithersburg, MD

Perkins NS (1950) Predicting exterior plywood performances. In: Proceedings of the National annual
    meeting. 4, 352–364. Forest Product Res Soc Portland, OR

Reiterer A, Sinn G, Stanzl-Tschegg S (2002a) Fracture characteristics of different wood species under
    mode I loading perpendicular to the grain. Mater Sci Eng, A 332(1–2):29–36

Reiterer A, Burgert I, Sinn G, Tschegg S (2002b) The radial reinforcement of the wood structure and its
    implication on mechanical and fracture mechanical properties—a comparison between two tree
    species. J Mater Sci 37(5):935–940

River BH (1994) Fracture of adhesive-bonded wood joints. In: Pizzi A, Mittal KL (eds) Handbook of
    adhesive technology. Marcel Dekker, New York, NY, pp 151–177

Schniewind AP, Centeno JC (1973) Fracture toughness and duration of load factor I. Six principal
    systems of crack propagation and the duration factor for cracks propagating parallel to grain. Wood
    Fiber 5:152–159

Sela N, Ishai O, Banks-Sills L (1989) The effect of adhesive thickness on interlaminar fracture toughness
    of interleaved CFRP specimens. Composites 20(3):257–264

Sinha A (2010) Effect of elevated temperature on mechanical behavior of structural wood and wood-
    based composites. Ph.D. thesis, Oregon State Univ., Corvallis, OR

Sinha A, Nairn JA, Gupta R (2011) Thermal degradation of bending strength of plywood and oriented
    strand board: a kinetics approach. Wood Sci Technol 45(2):315–330

Smith I, Vasic S (2003) Fracture behavior of softwood. Mech Mater 35:803–815

Smith I, Landis E, Gong M (2003) Fracture and fatigue in Wood. Wiley, West Sussex PO19 8SQ, England, pp 161–166

Stanzl-Tschegg SE, Navi P (2009) Fracture behavior of wood and its composites. A review. Holzforschung 63:139–149

Thuvander F, Berglund L (2000) In situ observations of fracture mechanisms for radial cracks in wood. J Mater Sci 35:6277–6283

Vasic S (2000) Applications of fracture mechanics to wood. Doctoral thesis, University of New Brunswick, New Brunswick, Canada

Wu EM (1963) Application of fracture mechanics to orthotropic plates. T&AM Report No. 248, department of theoretical and applied mechanics, University of Illinois, Urbana, Illinois

Wu EM (1967) Application of fracture mechanics to anisotropic plates. J Appl Mech 34(4):967–974

Yeh B, Schniewind AP (1992) Elasto-plastic fracture mechanics of wood using J integral method. Wood Fiber Sci 24(3):364–376

Yoshihara H, Nobusue K (2008) Mode I and Mode II fracture toughness of densified Sitka spruce fabricated in an airtight atmosphere with high temperature steam. Holzforschung 62:82–85

Zamborie BG, Kamke FA, Watson LT (2001) Simulation of the mat formation process. Wood Fiber Sci 33(4):564–579